ISSN 1063-7850, Technical Physics Letters, 2024. © Pleiades Publishing, Ltd., 2024.

Structural Change in Co–Cr–Fe–Mn–Ni Alloys upon Variation in Mn and Fe Concentrations

I. A. Panchenko[a,*], V. K. Drobyshev[a,], S. V. Konovalov[a,***], and D. A. Bessonov[a,****]**

[a]*Siberian State Industrial University, Novokuznetsk, 654007 Russia*

**e-mail: i.r.i.ss@yandex.ru*

***e-mail: drobyshev_v.k@mail.ru*

****e-mail: konovalov@physics.sibsiu.ru*

*****e-mail: dabess@narod.ru*

Received March 17, 2024; revised March 25, 2024; accepted March 25, 2024

Abstract—Co–Cr–Fe–Mn–Ni alloys with a change in the manganese and iron concentrations from 5 to 35 at % providing the optimum ratio between the strength and ductility have been investigated. Using a comprehensive study of the structure and mechanical properties of the samples, data on the effect of the elemental composition on the micro- and nanohardness of the Co–Cr–Fe–Mn–Ni alloys have been obtained and an optimum Mn-to-Fe ratio ensuring high strength has been determined. The structure and the phase and chemical compositions of the materials have been examined by X-ray diffraction analysis and scanning electron microscopy.

Keywords: high-entropy alloys, microhardness, nanohardness, electron microscopy, X-ray diffraction analysis, elemental mapping

DOI: 10.1134/S1063785024700391

INTRODUCTION

A conventional approach to creating structural materials consists in selecting a basic element as a matrix to obtain a desired combination of mechanical properties. In this way, a great number of alloys based on iron, copper, aluminum, etc., used in practice have been obtained. In recent years, the approach to creating multicomponent alloys with a matrix consisting of five or more elements in equiatomic ratios has evoked interest [1–7]. When alloys contain more than five elements, the entropy of mixing significantly increases, which is why they are called high-entropy alloys (HEAs). It is believed that high entropy facilitates the formation of disordered substitutional solid solutions instead of intermetallic phases due to a decrease in free energy. At present, it is known that the formation of the phase structure of HEAs is determined not only by the entropy of mixing (i.e., the number and concentration of constituents), but also by the nature of alloy components themselves. Among the most well-studied alloys based on transition elements, a single-phase structure of a disordered substitutional solid solution is only observed in the Co–Cr–Fe–Ni and Co–Cr–Fe–Ni–Mn alloys, while the formation of intermetallic or ordered phases is observed upon additional doping with many other elements. The aim of this study was to establish the effect of changes in the Mn and Fe concentrations on the structure and mechanical properties of the Co–Cr–Fe–Ni–Mn alloys and to determine formation criteria depending on changes in the manganese and iron contents.

MATERIALS AND METHODS

Six samples of Co–Cr–Fe–Mn–Ni HEAs with manganese and iron contents from 5 to 35 at % (Table 1) obtained by high-frequency induction melting were investigated.

The microhardness of the alloys was measured according to *GOST* (State Standard) 9450-76 using a diamond pyramid with a base angle of 136°, a load of

Table 1. Chemical composition of ingots (at %)

Alloy	Co	Cr	Fe	Mn	Ni
1	20	20	35	5	20
2	20	20	30	10	20
3	20	20	25	15	20
4	20	20	15	25	20
5	20	20	10	30	20
6	20	20	5	35	20

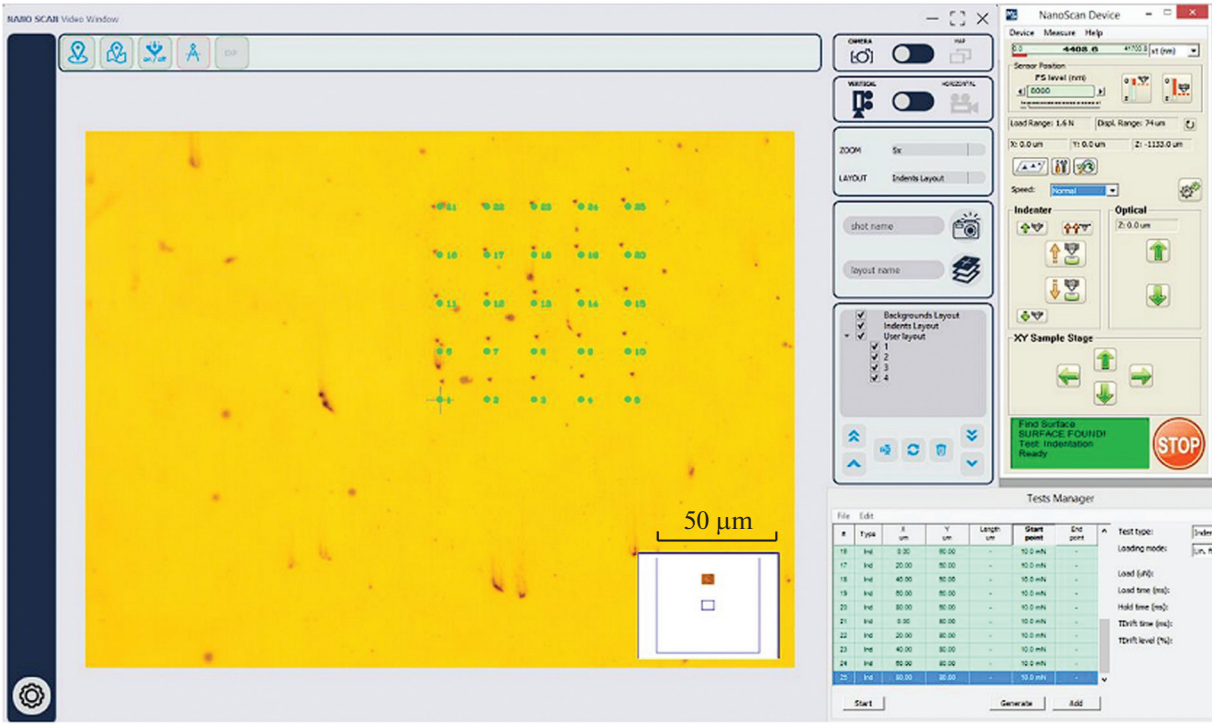

Fig. 1. Mesh of 5 × 5 indents with a load of 50 mN on the HEA samples.

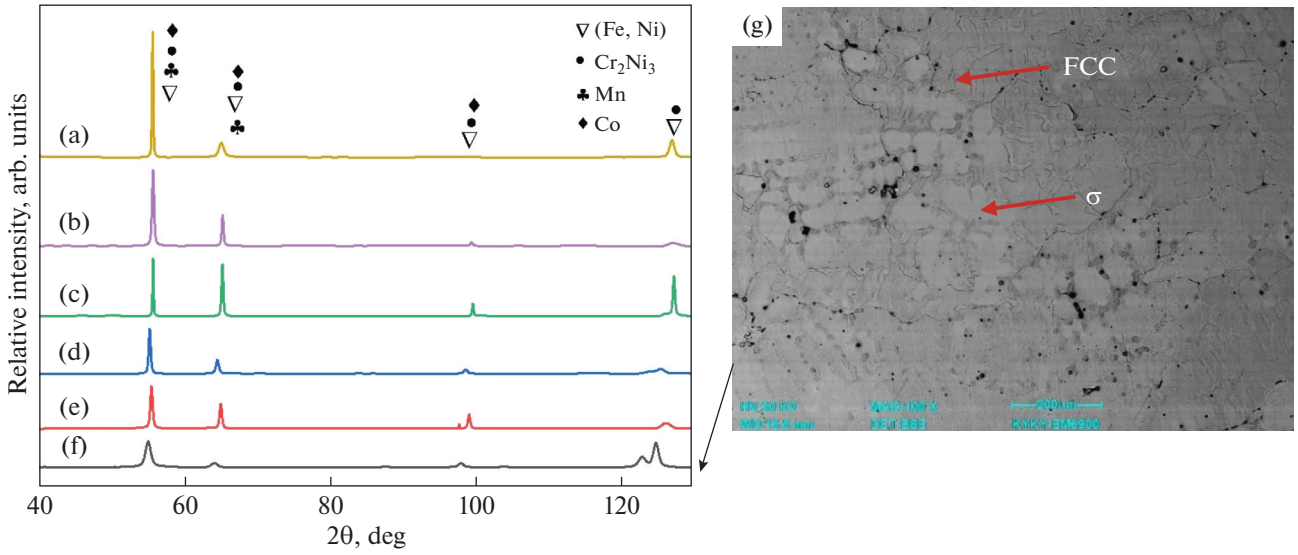

Fig. 2. XRD analysis of (a) $Co_{20}Cr_{20}Fe_{25}Mn_{15}Ni_{20}$, (b) $Co_{20}Cr_{20}Fe_{15}Mn_{25}Ni_{20}$, (c) $Co_{20}Cr_{20}Fe_{10}Mn_{30}Ni_{20}$, (d) $Co_{20}Cr_{20}Fe_5Mn_{35}Ni_{20}$, (e) $Co_{20}Cr_{20}Fe_{10}Mn_{30}Ni_{20}$, and (f) $Co_{20}Cr_{20}Fe_5Mn_{35}Ni_{20}$ alloys. (g) SEM image of $Co_{20}Cr_{20}Fe_5Mn_{35}Ni_{20}$ alloy obtained using a backscattered electron detector.

100 g, and an exposure time of 10 s. Nanoindentation of the alloys was carried out on a NanoScan-4D device according to the ISO 14577 and *GOST* (State Standard) R 8.748-2011 standards using a trihedral diamond pyramid (Berkovich indenter) with a blunt radius of about 20 nm at the apex; the distance between indents was 20 μm (Fig. 1).

Phases in the investigated alloys were identified by X-ray diffraction (XRD) analysis and scanning electron microscopy (SEM). XRD analysis was carried out using a diffractometer (Cu $K\alpha$ radiation). The microstructure was examined on a KYKY EM-6900 SEM at an accelerating voltage of 30 kV using both a classical secondary electron detector (SED) and a back-scattered electron detector (BSED) [8, 9]. When

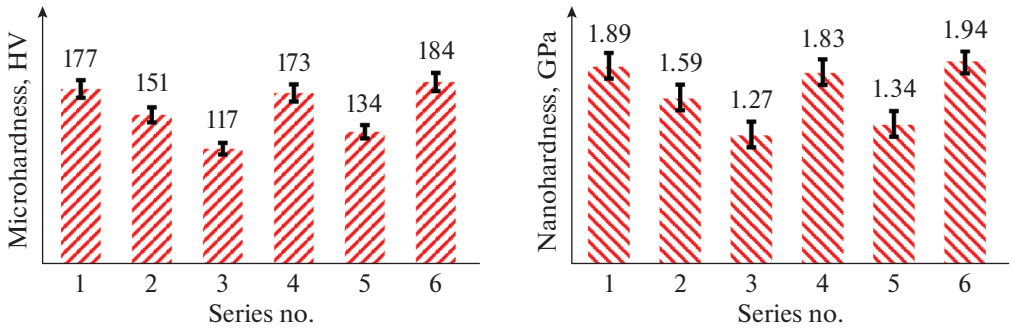

Fig. 3. Micro- and nanohardness data for Co–Cr–Fe–Mn–Ni alloys.

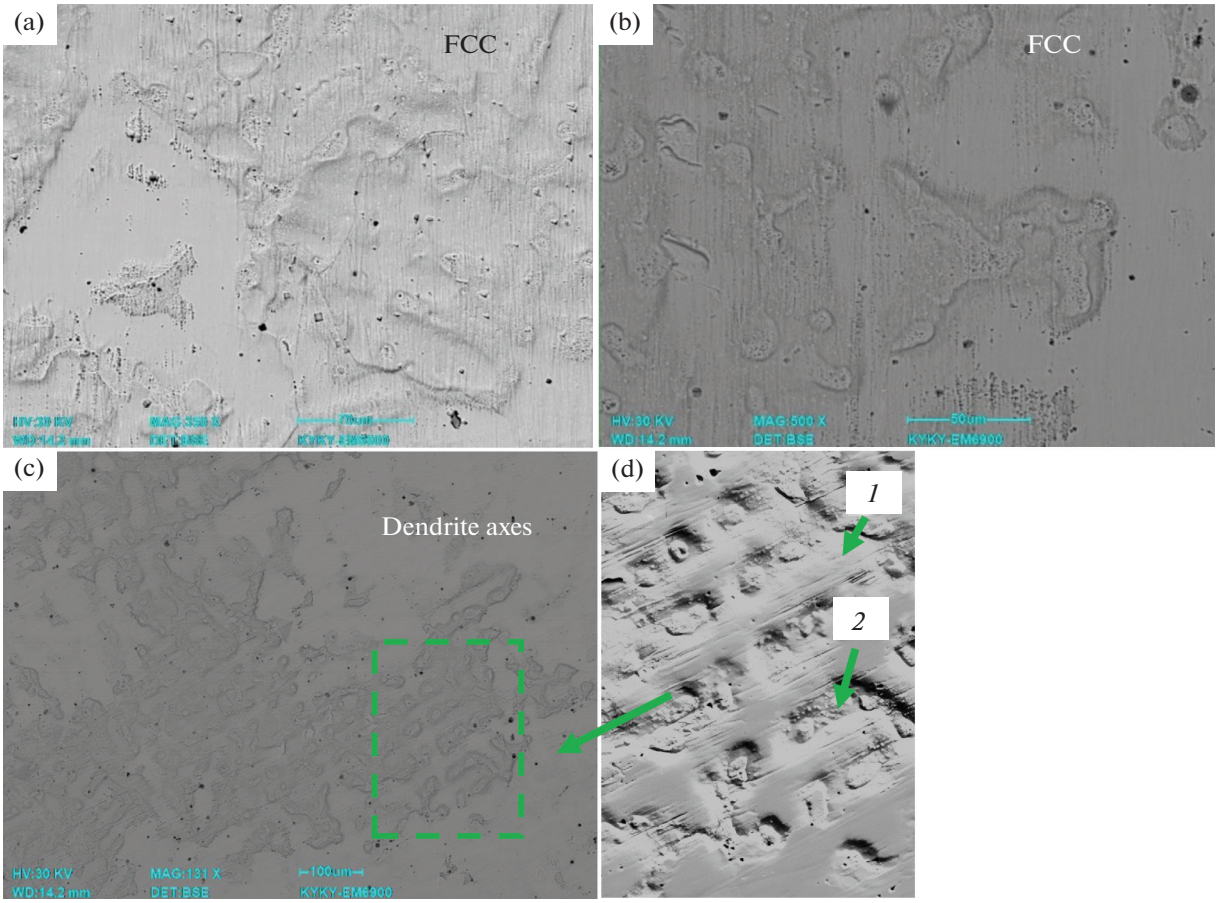

Fig. 4. Electron microscopy images of $Co_{20}Cr_{20}Fe_{10}Mn_{30}Ni_{20}$ alloy obtained at different magnifications with a backscattered electron detector.

using an SED, almost noiseless images with topographic contrast were obtained. When using a BSED with a working distance of up to 15 mm, the resulting images had a lower edge contrast, but brought information on the composition with a high sensitivity.

RESULTS AND DISCUSSION

XRD analysis (Fig. 2) showed that the presence of Mn greatly contributes to the formation of the structure of a solid solution, in contrast to the medium-entropy Co–Cr–Fe–Ni alloys [10]. The investigated alloys are single-phase solid solutions with an fcc lattice, which is fully consistent with the results of the study of the Cantor alloys with equiatomic contents of elements. The crystal lattice parameter was 3.6 ± 0.003 Å. An increase in the Mn content to 35 at % (Fig. 2) makes the crystal structure of the alloy more resistant to expansion and enhances the energy of fracture, which indicates a stronger interatomic bonding.

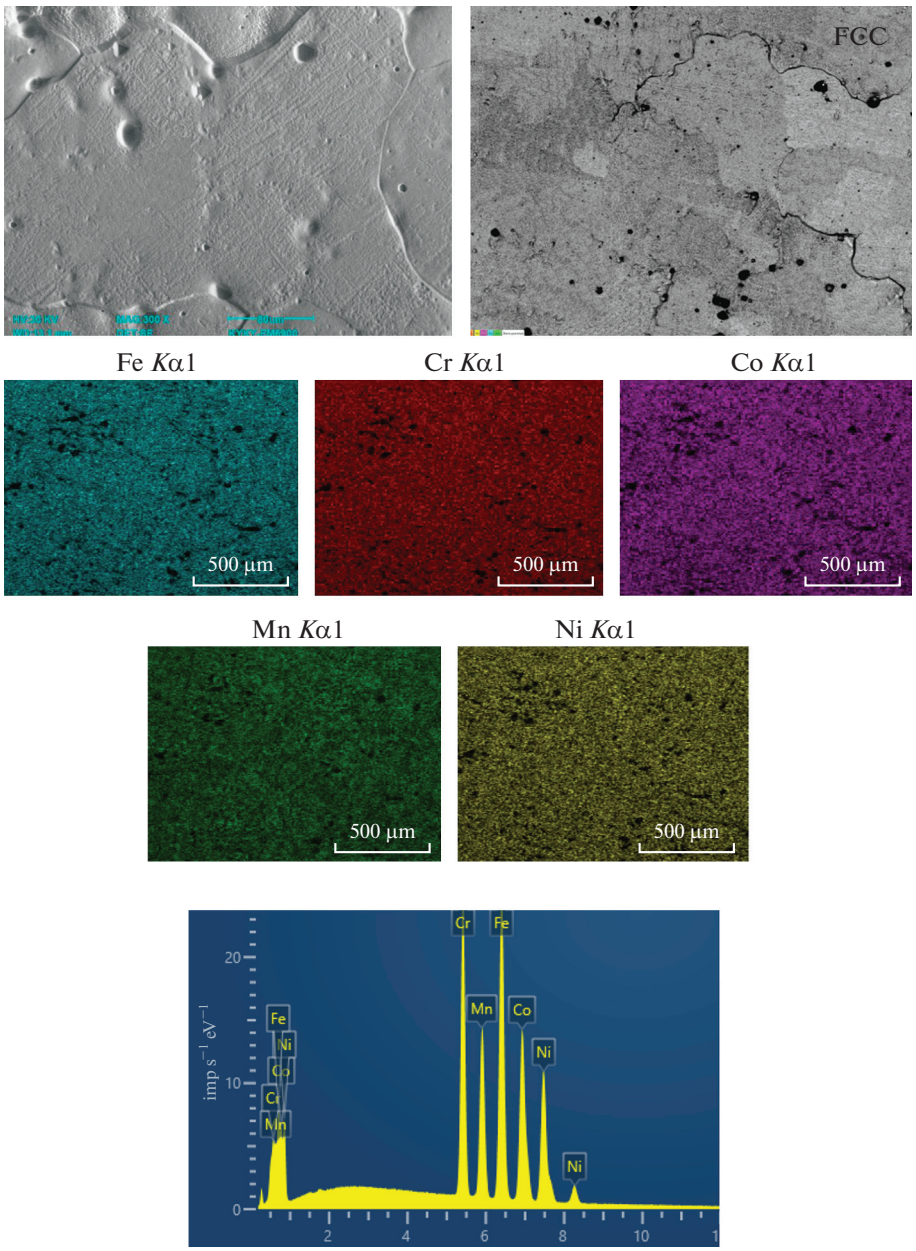

Fig. 5. Microstructure of $Co_{20}Cr_{20}Fe_{25}Mn_{15}Ni_{20}$ alloy visualized using secondary electron and backscattered electron detectors, elemental mapping, and energy spectra.

Table 2. Change in micro- and nanohardness depending on the elemental composition of the HEA

Series no.	Microhardness, HV	Nanohardness, GPa
1	177 ± 7	1.88 ± 0.06
2	151 ± 16	1.59 ± 0.32
3	117 ± 6	1.24 ± 0.06
4	173 ± 4	1.83 ± 0.115
5	134 ± 6	1.34 ± 0.04
6	184 ± 14	1.94 ± 0.12

Figure 2g shows a microphotograph of a $Co_{20}Cr_{20}Fe_5Mn_{35}Ni_{20}$ HEA obtained using a BSED. This alloy has the highest manganese content, due to which another strengthening intermetallic phase emerges in it.

Table 2 and Fig. 3 present the micro- and nanohardness data at different percentage of manganese and iron. The $Co_{20}Cr_{20}Fe_{35}Mn_5Ni_{20}$ and $Co_{20}Cr_{20}Fe_5Mn_{35}Ni_{20}$ alloys exhibited the highest hardness, which is confirmed by the results of the hardness and microhardness tests. The highest nanohardness (up to 1.94 GPa) can be caused by both an

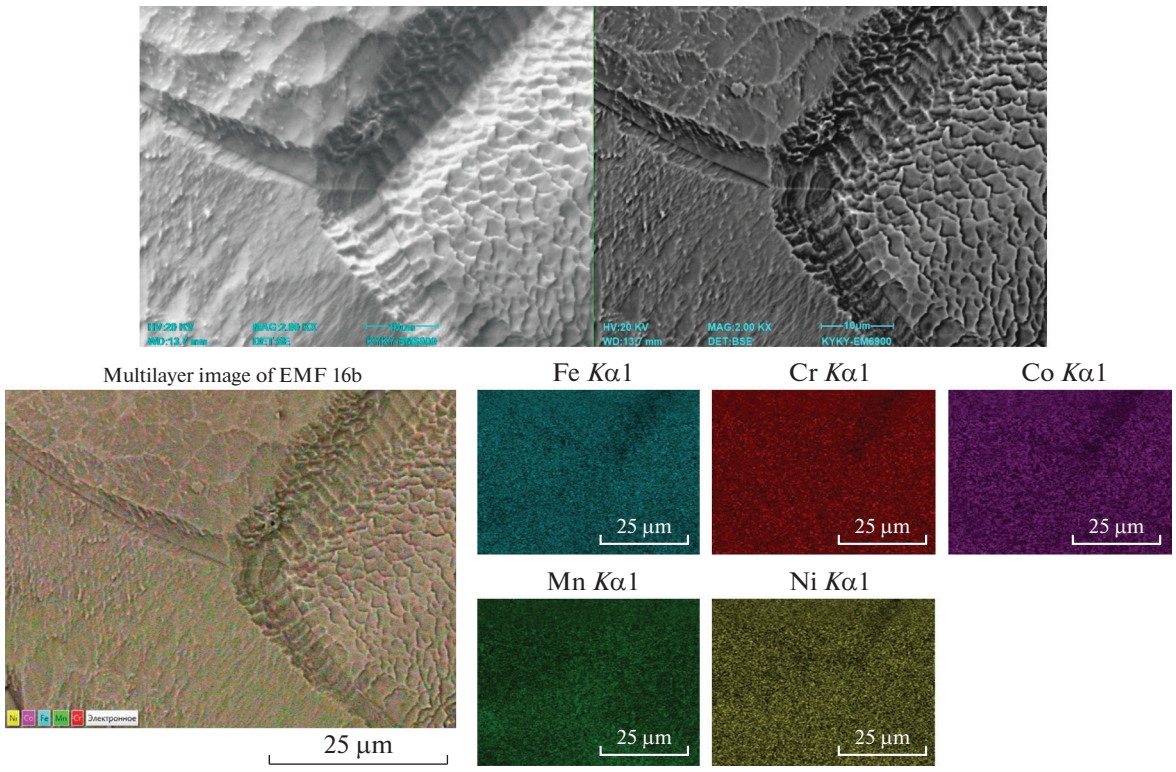

Fig. 6. SEM image of $Co_{20}Cr_{20}Fe_{25}Mn_{10}Ni_{20}$ alloy obtained with secondary electron and backscattered electron detector, elemental mapping, and energy spectra of the alloy region containing the interdendritic spacer.

increase in the manganese content to 35 at % for the $Co_{20}Cr_{20}Fe_5Mn_{35}Ni_{20}$ alloy and the presence of strengthening intermetallic phases (see the XRD data in Fig. 2f) for the $Co_{20}Cr_{20}Fe_{35}Mn_5Ni_{20}$ alloy.

To evaluate the structure of the alloy, Fig. 4 shows SEM images obtained with a detector that provides information about the composition of the examined area of the $Co_{25}Cr_{25}Fe_{10}Mn_{30}Ni_{20}$ alloy with a high sensitivity. It can be noted that this alloy represents a single-phase solid solution with an fcc lattice (Fig. 2e)

Table 3. Chemical composition of the dendritic region of $Co_{20}Cr_{20}Fe_{25}Mn_{10}Ni_{20}$ alloy

Total mapping spectrum

Element	Line type	wt %	Sigma wt %	at %
Cr	K series	18.69	0.06	20.17
Mn	K series	11.24	0.06	11.48
Fe	K series	29.38	0.08	29.59
Co	K series	20.75	0.08	19.76
Ni	K series	19.95	0.09	19.07
Total	K series	100.00		100.00

and a heterogeneous structure in the form of dendrite branches (Figs. 4a–4d). The first- and second-order dendrites can be seen, which are enriched with cobalt, chromium, and iron in the bulk of a grain and with manganese and nickel in the border areas (Figs. 4c, 4d).

The $Co_{20}Cr_{20}Fe_{25}Mn_{15}Ni_{20}$ alloy (Figs. 5, 6; Table 3) also has a simple single-phase structure (Fig. 2) consisting of simple disordered substitutional solid solutions with an fcc lattice. When studying the microstructure of this alloy, it is worth noting its dendritic segregation (Fig. 4), a high content of refractory elements in the dendritic regions (Table 3), and release of low-melting Ni and Mn elements in the interdendritic layers (Fig. 5). The average grain size was 200–300 μm; black globules 5–10 μm in size are nonmetallic inclusions of the Mn_2O_3 oxide.

CONCLUSIONS

(i) In this study, the presence of intermetallic phases in the $Co_{20}Cr_{20}Fe_5Mn_{35}Ni_{20}$ alloy positively affecting the mechanical properties was established, which is related to a high (up to 35 at %) Mn content. The remaining alloys are single-phase solid solutions with a fcc lattice parameter of 3.6 ± 0.003 Å.

(ii) The highest nanohardness among the investigated alloys was exhibited by the $Co_{20}Cr_{20}Fe_5Mn_{35}Ni_{20}$

and $Co_{20}Cr_{20}Fe_{35}Mn_5Ni_{20}$ samples: 1.88 ± 0.06 and 1.94 ± 0.12 GPa, respectively.

(iii) Using scanning electron microscopy, the structure of the materials was found to be dendritic segregation with a grain size of 200–300 μm and the presence of nonmetallic Mn_2O_3 inclusions was observed.

FUNDING

This study was supported by the Russian Science Foundation, project no. 23-49-00015 (https://rscf.ru/project/23-49-00015/).

CONFLICT OF INTEREST

The authors of this work declare that they have no conflicts of interest.

REFERENCES

1. B. S. Murty, J. W. Yeh, and S. Ranganathan, *High-Entropy Alloys* (Butterworth-Heinemann, 2014).
2. J.-W. Yeh, S.-K. Chen, S.-J. Lin, J.-Y. Gan, Ts.-Sh. Chin, T.-Ts. Shun, Ch.-H. Tsau, and Sh.-Y. Chang, Adv. Eng. Mater. **6** (8), 299 (2004).
3. J. W. Yeh, S. Y. Chang, Y. D. Hong, S. K. Chen, and S. J. Lin, Mater. Chem. Phys. **103**, 41 (2007).
4. K. Y. Tsai, M. H. Tsai, and J. W. Yeh, Acta Mater. **61** (13), 4887 (2013).
5. A. Gali and E. P. George, Intermetallics **39**, 74 (2013).
6. Z. Wang, I. Baker, W. Guo, and J. D. Poplawsky, Acta Mater. **126**, 346 (2017). https://doi.org/10.1016/j.actamat.2016.12.074
7. Z. Li, Acta Mater. **16**4, 400 (2019). https://doi.org/10.1016/j.actamat.2018.10.050
8. P. Stutzman, Cem. Concr. Compos. **26** (8), 957 (2004). https://doi.org/10.1016/j.cemconcomp.2004.02.043
9. M. A. F. Eres, F. M. Valle-Algarra, J. V. G. Adelantado, et al., Microchim. Acta **162** (3-4), 341 (2008). https://doi.org/10.1007/s00604-007-0926-5
10. Liu Yu, Liu Wei, Zhou Qiong, Liu Chao, Fan Tou-Wen, Wu Yuanqi, Wang Zhipeng, and Tang Ping, J. Mater. Res. Technol. **17**, 498 (2022). https://doi.org/10.1016/j.jmrt.2022.01.013

Translated by E. Bondareva